The Astrophysical Journal Letters, 815:L30 (5pp), 2015 December 20 doi:10.1088/2041-8205/815/2/L30

ON THE DIFFERENTIAL ROTATION OF MASSIVE MAIN-SEQUENCE STARS

T. M. Rogers
Department of Mathematics and Statistics, Newcastle University, UK
Planetary Science Institute, Tucson, AZ 85721, USA
Received 2015 September 28; accepted 2015 November 10; published 2015 December 18

ABSTRACT

To date, asteroseismology has provided core-to-surface differential rotation measurements in eight main-sequence stars. These stars, ranging in mass from $\sim$1.5–9 $M_{\odot}$, show rotation profiles ranging from uniform to counter-rotation. Although they have a variety of masses, these stars all have convective cores and overlying radiative regions, conducive to angular momentum transport by internal gravity waves (IGWs). Using two-dimensional numerical simulations, we show that angular momentum transport by IGWs can explain all of these rotation profiles. We further predict that, should high mass, faster rotating stars be observed, the core-to-envelope differential rotation will be positive, but less than one.

Key words: asteroseismology – stars: rotation – waves

1. INTRODUCTION

Rotation is a key property of stars that has important consequences for their long-term evolution and eventual demise. Rotation is particularly important in massive stars where it contributes significantly to chemical mixing (Zahn 1992; Talon et al. 1997) and may determine the eventual explosion energy and nucleosynthetic yield of the star (Heger & Langer 2000). Given its importance, it would be extremely beneficial if constraints could be placed on stellar internal rotation as well as on the dominant physical mechanisms responsible for such rotation. However, theoretically determining the internal rotation of stars is plagued by complicated hydrodynamic processes, which are difficult to simulate numerically and, until recently, observations have provided little constraint.

Fortunately, the observational landscape has recently changed due to space missions like Convection, Rotation and planetary Transits (CoRoT), and *Kepler*. With the continuous duty cycle provided by these missions, observers have been able to place constraints on the internal rotation of hundreds of evolved stars using mixed modes (Beck et al. 2012; Mosser et al. 2012; Deheuvels et al. 2015). The overall consensus of these observations is that angular momentum coupling between the contracting core and envelope is far more efficient than previously expected. Although it is still unclear what the physical mechanism is that causes this efficient coupling, internal gravity waves (IGWs) are key contenders (Fuller et al. 2014).

Core-envelope differential rotation has also been measured in eight intermediate and massive main-sequence stars using both p- and g-modes (Aerts et al. 2003; Pamyatnykh et al. 2004; Briquet et al. 2007; Kurtz et al. 2015; Saio et al. 2015; Schmid et al. 2015; Triana et al. 2015). We note that the term core here is used to mean the region just outside the convective core and is really the inner radiative region. Throughout this text, we will use this terminology for consistencies sake but emphasize that "core" used here does *not* refer to the *convective* core. This handful of observations has shown a variety of differential rotation profiles. The measurements of HD 157056 (Briquet et al. 2007), KIC 9244992 (Saio et al. 2015), KIC 11145123, (Kurtz et al. 2015), and the binary system KIC 10080943 (Schmid et al. 2015) show fairly uniform rotation, although notably not *exactly* uniform. On the other hand, HD 29248 (Pamyatnykh et al. 2004) and HD 129929 (Aerts et al. 2003) show cores spinning more rapidly than their envelopes. Finally, HD 10526294 (Triana et al. 2015) shows an envelope spinning faster than the core and in the opposite direction.

It has been shown previously that IGWs generated by convection are very efficient at transporting angular momentum (Rogers et al. 2013). This is particularly true in stars that have convective cores and extended overlying radiative regions. In this configuration, IGWs generated at the convective–radiative interface propagate outward into a region whose density is decreasing dramatically. This causes wave amplitudes to increase rapidly. Because of this increase in amplitude, very small amplitude perturbations at generation can lead to large perturbations in the envelope and, therefore, lead to efficient angular momentum transport if the waves dissipate (Rogers et al. 2013).

Convection generates both prograde and retrograde waves at the convective–radiative interface. The initial symmetry breaking of a uniformly rotating medium caused by the dissipation of predominantly prograde or retrograde waves at the surface is a stochastic process, meaning the angular momentum transport by IGWs could either speed up (if prograde waves are dissipated) or slow down (if retrograde waves are dissipated) the radiative region.

This initial symmetry breaking sets the stage for further angular velocity evolution, which will depend on the dominant dissipation mechanism. If waves dissipate through nonlinear wave breaking, then subsequent evolution can vary in sign and a strong mean flow may not develop. If waves dissipate predominantly through radiative dissipation then whichever sign flow dominates initially will grow and eventually reverse in time (as in the Quasi-Biennial Oscillation (Baldwin et al. 2001), though it is still unclear whether such an oscillation would proceed in a massive star (Rogers et al. 2013)). Similarly, if a critical layer develops, then any initial mean flow will be amplified, but on a much faster timescale (than radiative diffusion alone). In massive stars, the density stratification is such that waves are likely to nonlinearly break. However, whether or not a critical layer develops will depend on the surface wave flux, which depends on the convective

flux, and the details of the stratification. Therefore, the outcome of IGW transport can vary from simple efficient angular momentum transport between the convective and radiative regions, to strong differential rotation if a critical layer develops.

While the observed stars vary in mass, they share the common characteristic of having convective cores with overlying radiative regions, albeit with different extent. Given the limited number and resolution of the observations, here we use a single fiducial model of a star with a convective core and radiative envelope. By simply varying the initial rotation rate (to mimic different initial conditions) and convective flux (to mimic different masses and ages), we show that angular momentum transport by convectively driven IGWs can explain the variety of observed rotation profiles.

2. OBSERVATIONS OF CORE-ENVELOPE DIFFERENTIAL ROTATION IN MASSIVE MAIN-SEQUENCE STARS

To date, core-envelope differential rotation has been measured in eight main-sequence intermediate and massive stars. Here we briefly summarize those results. The first measurement of core-envelope differential rotation (Ω_c/Ω_e) in a main-sequence star was done by Aerts et al. (2003) for the B3V star HD 129929. That star was found to have a core rotating approximately 3.6 times faster than its envelope (Dupret et al. 2004; Aerts 2008). HD 29248, another B star of similar mass (Ausseloos et al. 2004; Pamyatnykh et al. 2004), was found to have a core spinning approximately five times faster than its envelope. Briquet et al. (2007) found a rotation profile consistent with uniform rotation for the $\sim 8\,M_\odot$ star HD 157056. More recently, Kurtz et al. (2015) and Saio et al. (2015) have found nearly uniform rotation for the F stars KIC 9244992 and KIC 11145123. Though, importantly, with high confidence, they find that KIC 9244992 has an envelope rotating slightly slower than its core ($\Omega_c/\Omega_e = 0.97$) and conversely KIC 11145123 has an envelope spinning slightly faster than its core ($\Omega_c/\Omega_e = 1.03$). Similarly, Schmid et al. (2015) constrained core-envelope differential rotation in both components of the binary system KIC 10080943 and found that one object has a slightly faster core than envelope, while the other member shows the opposite.[1] Finally, Triana et al. (2015) used 19 g-mode multiplets to do a full inversion to find the radial differential rotation profile for KIC 10526294. They found that the envelope was spinning significantly faster than the core ($\Omega_c/\Omega_e = 0.3$) but, perhaps more surprising, with the opposite sign. That is, the envelope is rotating in the opposite direction to the core, see Figure 3.

With the exception of Triana et al. (2015), all of these stars only have a measurement of the ratio of Ω_c/Ω_e and not an actual rotation profile. These ratios are derived from multiplets of g-modes, which are confined to the region just outside of the convection zone, and multiplets of p-modes, which are confined to the surface regions. Therefore, the differential rotation measurement is really a measure of two regions of the star, just outside the convective core and just beneath the surface. Furthermore, mode identification is much easier in slower rotators, therefore, all of the observed stars are slow rotators, perhaps unusually so. Therefore, these observed stars may not represent the rotation profiles of intermediate and massive main-sequence stars as a whole. Consequently, in the following, we will consider a variety of initial rotation rates.

[1] It is very likely that *tidally induced* waves, which we do not consider here, could contribute to this rotation profile.

3. MODELING ANGULAR MOMENTUM TRANSPORT BY IGWs

In order to model angular momentum transport by IGWs in stellar interiors, we solve the Navier–Stokes equations in the anelastic approximation (Gough 1969; Rogers & Glatzmaier 2005). The equations are solved in two dimensions, representing an equatorial slice of the star. Here we use a $3\,M_\odot$ star as a fiducial model. The radial domain extends from $0.01\,R_\star$ to $0.90\,R_\star$, encompassing both the convective core and radiative envelope to accurately model the convective generation of waves. The reference state thermodynamic variables are calculated from a polynomial fit to a one-dimensional model calculated using the Cambridge stellar evolution code STARS for a $3\,M_\odot$ star (Eggleton 1971), with a central hydrogen fraction, $X_c = 0.47$. At this age, the convective core occupies $0.30\,R_\odot$ or 14% of the radial domain. Because of the steep density gradient 90% of the angular momentum of the star resides within 60% of the radius.

These simulations, like all hydrodynamic simulations, require higher than realistic diffusion coefficients for numerical stability (here we use $\nu = 4 \times 10^{13}$ and $\kappa = 5 \times 10^{11}\,\mathrm{cm^2\,s^{-1}}$). Such diffusion coefficients would damp IGWs unrealistically on their journey to the surface of the star. To compensate for this enhanced diffusion, we force the waves harder by forcing the convection harder so that the waves reach the surface with more realistic amplitudes. Forcing the convection harder leads to convective velocities, which are ~10–20 times larger than expected from mixing-length theory, depending on the model. However, if we compare our simulated surface velocities to those calculated assuming mixing length theory for the convective velocities, proper density stratification, and realistic diffusivities, those velocities are comparable. More details of the numerical model can be found in Rogers et al. (2013).

Because the observations span a range of masses, here we consider slightly different convective fluxes as a crude way to mimic different stellar masses and ages. Broadly, we expect higher convective fluxes (Q/c_v) to be associated with more massive stars, but given the other details we have neglected, such as varying stratification and age, this is not necessarily the case. We further consider different rotation rates to mimic different initial conditions. Table 1 lists the initial conditions and parameters of the models considered along with their resulting core-envelope differential rotation. Figure 1 shows a typical time snapshot within the simulated domain of the temperature and vorticity for model M4.

4. SIMULATED CORE-ENVELOPE DIFFERENTIAL ROTATION

To mimic the regions probed by observations, we average the core rotation over $\sim 0.2\,R_\star$ outside the convection zone (Ω_c) and the surface rotation over $\sim 0.1\,R_\star$ below the surface (Ω_e). The ratio of these two values varies substantially in time; therefore, to best illustrate the results, we show the histogram of values obtained for each model in Figure 2 (details are in the figure caption). The distribution of values seen in Figure 2 indicates the stochastic nature of wave generation and dissipation. Hence, while most of the profiles are Gaussian with a clear average,

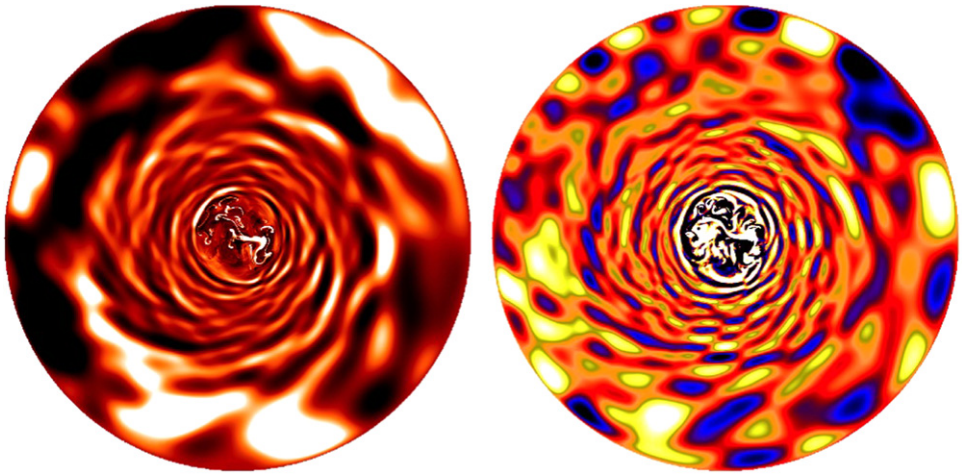

Figure 1. Time snapshot of M4. (Left) Temperature perturbation with white hot and black cool perturbations. (Right) Vorticity with black negative vorticity and white positive.

Table 1
Model Parameters

Model	Ω_i (rad s^{-1})	$\overline{Q}/c_v$	Ω_c/Ω_e	$\langle AM\rangle/AM_i$
M1	10^{-7}	1.5	2.5 ± 2.3	1.005
M2	5×10^{-7}	1.5	0.5 ± 1.9	1.021
M3	10^{-6}	1.5	3.73 ± 3.46	1.010
M4	10^{-6}	3.0	−0.06 ± 0.14	1.021
M5	5×10^{-6}	1.5	0.60 ± 0.81	0.998
M6	5×10^{-6}	2.2	1.24 ± 1.56	1.020
M7	5×10^{-6}	3.0	−0.14 ± 0.65	0.990
M8	10^{-5}	1.5	1.06 ± 0.34	1.000
M9	10^{-5}	3.0	0.20 ± 0.11	1.010
M10	4×10^{-5}	1.5	0.97 ± 0.10	1.001
M11	4×10^{-5}	3.0	0.21 ± 0.18	1.008
M12	8×10^{-5}	1.5	0.93 ± 0.06	1.000
M13	8×10^{-5}	3.0	0.12 ± 0.03	1.011

Note. Ω_i is the initial rotation rate given in rad s^{-1}. $\overline{Q}/c_v$ represents the convective forcing in units K s^{-1}, where c_v is the specific heat at constant volume. The values 1.5 and 3 result in root-mean-squared convective velocities of ∼2.9 and 4.5 km s^{-1}, respectively, values ∼10 and ∼20 times larger than predicted by mixing length theory. The differential rotation, Ω_c/Ω_e, represents the mean ratio of core-to-envelope rotation. The time and spatial averaging are discussed in the text. Errors quoted are due to variations in time, which are also discussed in the text. $\langle AM\rangle/AM_i$ represents the integrated angular momentum compared to the initial angular momentum content of the system, demonstrating the level at which angular momentum is conserved in the system.

there is some deviation and skewness. The values of Ω_c/Ω_e quoted in Table 1 are the mean values with errors of one standard deviation. The variability due to differences in spatial averaging are smaller than those in time, so long as Ω_c is measured within the radiative region and away from convective overshoot. If the core value includes the convection zone, the ratio Ω_c/Ω_e becomes significantly more variable, tends to increase and its distribution is often not Gaussian. This may be due to inadequate time resolution or reduced dimensionality, but is more likely due to the stochastic nature of turbulent convection. Each of the models is run for at least 20 wave crossing times of the entire radiative envelope for a typical wave (horizontal wavenumber 10 and frequency 10 μHz), or ∼100 convective turnover times, which amounts to $\sim 10^7$ s. We note that some models are run substantially longer and do not show substantial variation and certainly none outside the error bars quoted.

In Figure 2, we immediately see that the range of differential rotation profiles seen in the simulations (−0.03–5) is similar to that observed (−0.3–5). More specifically, our low flux models with a variety of low rotation rates converge to core-envelope differential rotation values between ∼1–5, similar to seven of the eight observations of differential rotation (HD 129929, HD 29248, HD 157056, KIC 9244992, KIC 11145123, KIC 10080943). These models show a slight preference toward values closer to one than to five, similar to the observations. Simply, we expect HD 129929, HD 29248, and HD 157056 to be described by high flux rather than low flux models. However, numerous other effects (such as stratification, Brunt–Vaisala barrier, etc.—see the Discussion) could affect the surface flux of waves contributing to these stars appearing more like low flux models. Low flux, high rotation models also show values very close to one. Notably though, the averages are not exactly one. Therefore, in these low flux models, there is some angular momentum transport by waves but not enough to bring the system significantly away from its initially uniform state. This is particularly true in faster rotating models, where wave transport is less efficient.

High flux models, on the other hand, converge to core-envelope differential rotation values generally between ±1. In this case, IGWs are particularly efficient at spinning up (in amplitude) the radiative envelopes and hence, envelopes generally spin faster than cores. For slow rotators this transport is efficient enough and predominantly due to retrograde waves, so that negative values are common. On the other hand, in fast rotators, prograde waves dominate and bring about a fast, but positive rotation in the envelope. It is worth noting that, in general, slow rotators tend to favor retrograde wave deposition at the surface and hence, retrograde envelope rotation, while fast rotators favor prograde wave deposition at the surface and hence, prograde envelope rotation. At the moment, the theoretical reason for this tendency is unknown.

The high flux, slow rotator behavior seen in these simulations is similar to the differential rotation pattern observed in the star KIC 10526294 (Triana et al. 2015). In Figure 3, we show the rotation profile inferred for KIC 10526294 (Triana et al. 2015), with error bars, along with time-averaged rotation profiles from M4, which was initiated with a rotation rate similar to

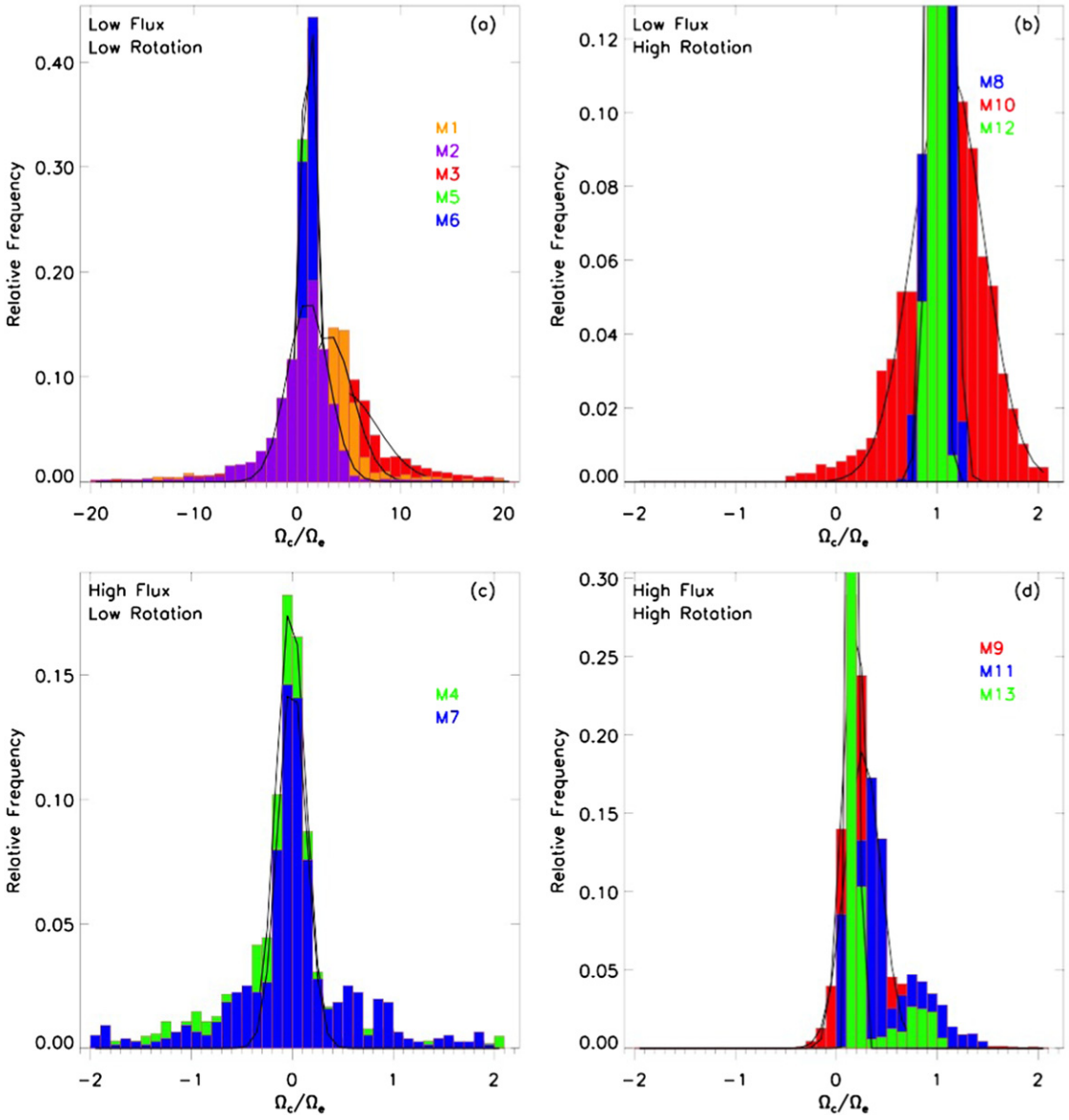

Figure 2. Histogram of Ω_c/Ω_e for models listed in Table 1. (a) Low flux, low rotation models M1, M2, M3, M5, M6. Mean values range from ∼0.5 to ∼4. In general, these models could explain the rotation measurements of HD 129929, HD 29248, HD 157056, KIC 9244992, KIC 11145123, and KIC 10080943. (b) Low flux, high rotation models M8, M10, M12. Such stars have not yet been observed. Ratios are ∼1, IGW transport some angular momentum, but not so much to bring about substantial differential rotation. (c) High flux, low rotation models M5 and M8. In these models IGW transport significant angular momentum, causing the envelope to spin substantially faster than the core. In these low rotation models, negative ratios (envelope spinning retrograde) are favored, nicely explaining the observation of Triana et al. (2015). (d) High flux, high rotation models M9, M11, and M13. IGW transport is efficient enough to cause the envelope to spin faster than the core, so that $\Omega_c/\Omega_e < 1$, but in contrast to the slowly rotating models, these favor positive (prograde) surface rotation. Again these stars have yet to be observed.

KIC 10526294 and which develops a counter-rotating envelope. There we see that a low rotation model with high IGW flux could reproduce the observed rotation profile of KIC 10526294. The outer layers of the star, that are spinning retrograde, represent only ∼1% of the angular momentum. Therefore, those models that only conserve angular momentum to ∼2% might not accurately capture the surface dynamics. However, in this particular case (M4), the angular momentum is *larger* than the original value, so the angular momentum discrepancy cannot be explained by the retrograde envelope. Therefore, while we have to be careful when interpreting our surface angular velocities, this likely does not affect these particular results. We should note that while our time averaged Ω_c/Ω_e are similar to observed values it is worth keeping in mind that observations represent an instant in time, not a time average, so any of the values seen in Figure 2 could potentially be observed. Similarly, while we have been able to reproduce the rotation profile of KIC 10526294 with a time averaged profile, we expect that run long enough, our simulated profile would evolve.

5. DISCUSSION

Based on these two-dimensional (2D) numerical simulations, we conclude that IGWs can explain current observations of core-envelope differential rotation in main-sequence stars with a convective core. These results lead to a few conclusions and predictions. Low flux models with low rotation can show a variety of differential rotation profiles, ranging from ∼1–5. Low flux models with high rotation have rotation profiles

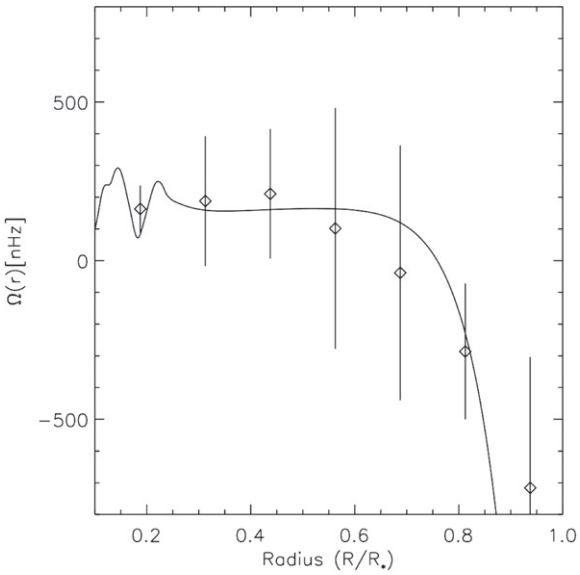

Figure 3. Angular velocity as a function of radius for KIC 10526294 as measured by Triana et al. (2015; diamonds connected by solid line) with vertical lines indicating error bars. Time average of the angular velocity from Model M4 is shown overlaid.

closer to uniform, though notably, not exactly. High flux models with low rotation generally show faster and counter-rotating envelopes. Finally, high flux models of high rotation (which have not yet been observed) will have envelopes spinning faster than their core, but with positive sign. In our simulations the transition between fast and slow rotators (or retrograde versus prograde envelopes) occurs $\sim 10^{-5}$ rad s^{-1}, but this will likely depend on the age and mass of the star.

Given that simply changing the convective flux by a factor of two in our simulations can lead to significantly different rotation profiles it is worth discussing what could lead to a different convective flux in a real star, or more appropriately, a different surface wave flux. Of course, the first is mass, with higher mass stars having higher luminosities and, therefore, higher convective fluxes. The second is age, as a star evolves its luminosity increases somewhat, which could lead to enhanced convective fluxes. However, as the star ages it also develops a severe gradient in the Brunt–Vaisala frequency at the convective–radiative interface due to the chemical composition gradient left behind by converting hydrogen to helium. Such a gradient could act as a filter to waves propagating outward to the surface and thus reduce the surface wave flux, possibly causing a massive star to appear more like a low flux model. It is hard to know how these two effects combined affect the surface wave flux. In reality, changes in both mass and age are also accompanied by changes in the stratification throughout the radiative region, which could affect the effective propagation and dissipation of waves, and hence the wave flux. Any of these effects could contribute to individual stars being better described by different model parameters than initially expected and all of these effects should be considered in future models and as more observations become available.

This work, in addition to Aerts & Rogers (2015), is one of the first to make direct comparisons between numerical hydrodynamic simulations and observations. Such comparisons clearly require some caveats. First and foremost, these simulations are carried out in two dimensions. We expect that IGW transport would be more efficient in two dimensions because waves are not able to spread out over the sphere and because 2D turbulence has an inverse cascade. Therefore, we expect the timescales of angular momentum transport in these simulations to be shorter than in the actual star, but we cannot say by how much. This difficulty in extrapolating timescales is because mean flow development depends on velocity correlations and it is difficult to say how much more efficient these correlations are in two dimensions versus three dimensions. Furthermore, we do not know how wave transport will proceed at higher latitudes but we expect it to be less efficient than at the equator. Therefore, the observations, which represent a latitudinal average, are likely a lower limit of our simulated equatorial differential rotation. Finally, treating mass and evolutionary state as simply a change in flux is inadequate. As observations become more plentiful, future simulations will be more precise.

We have shown that our numerical simulations of IGWs can explain the observed differential rotation profiles observed in intermediate and massive main-sequence stars. Given the shortcomings of these simulations (2D, increased viscosity, increased thermal diffusivity) it is surprising that the results agree as well as they do. This agreement is likely due to the limited observational constraints and to the fact that IGW transport can vary significantly. As observational constraints become more numerous, more sophisticated simulations, which properly consider mass and age of individual stars and proper dimensionality, will be necessary. In turn, we expect that additional observational constraints can be used to constrain simulation parameters. One robust conclusion from both the observations and the numerical simulations is that stellar rotation is complex and can admit a variety of profiles.

Support for this research was provided by NASA grant NNX13AG80G to T.R. Computing was carried out on Pleiades at NASA Ames. T.R. would like to thank an anonymous referee for insightful and helpful comments, which improved this manuscript significantly. She would also like to thank C. Aerts, S. Triana, and E. Morraveji for useful conversations leading to the development of this manuscript.

REFERENCES

Aerts, C. 2008, in Proc. IAU Symp 250, Massive Stars as Cosmic Engines (Cambridge: Cambridge Univ. Press), 237
Aerts, C., & Rogers, T. M. 2015, ApJL, 806, L33
Aerts, C., Thoul, A., Daszyńska, J., et al. 2003, Sci, 300, 1926
Ausseloos, M., Scuflaire, R., Thoul, A., & Aerts, C. 2004, MNRAS, 355, 352
Baldwin, M. P., Gray, L., Dunkerton, T. J., et al. 2001, RvGeo, 39, 179
Beck, P. G., Montalban, J., Kallinger, T., et al. 2012, Natur, 481, 55
Briquet, M., Morel, T., Thoul, A., et al. 2007, MNRAS, 381, 1482
Deheuvels, S., Ballot, J., Beck, P. G., et al. 2015, A&A, 580, 96
Dupret, M. A., Thoul, A., Scuflaire, R., et al. 2004, A&A, 415, 251
Eggleton, P. P. 1971, MNRAS, 151, 351
Fuller, J., Lecoanet, D., Cantiello, M., & Brown, B. 2014, ApJ, 796, 17
Gough, D. O. 1969, JAtS, 26, 448
Heger, A., & Langer, N. 2000, ApJ, 544, 1016
Kurtz, D. W., Shibahashi, H., Murphy, S. J., Bedding, T. R., & Bowman, D. M. 2015, MNRAS, 444, 102
Mosser, J., Goupil, M. J., Belkacem, K., et al. 2012, A&A, 548, 10
Pamyatnykh, A. A., Handler, G., & Dziembowski, W. A. 2004, MNRAS, 350, 1022
Rogers, T. M., & Glatzmaier, G. A. 2005, ApJ, 620, 432
Rogers, T. M., Lin, D. N. C., McElwaine, J. N., & Lau, H. H. B. 2013, ApJ, 772, 26
Saio, H., Kurtz, D. W., Takata, M., et al. 2015, MNRAS, 447, 3264
Schmid, V. S., Tkachenko, A., Aerts, C., et al. 2015, A&A, in press
Talon, S., Zahn, J. P., Maeder, A., & Meynet, G. 1997, A&A, 209, 322
Triana, S. A., Moravveji, E., Papics, P. I., et al. 2015, ApJ, 810, 16
Zahn, J. P. 1992, A&A, 265, 115